Generalized Vicsek Fractals: Regular Hyperbranched Polymers

A. Blumen,[†] Ch. von Ferber,[†] A. Jurjiu,[†] and Th. Koslowski*[,‡]

Theoretische Polymerphysik, Universität Freiburg, Hermann-Herder-Strasse 3, D-79104 Freiburg, Germany, and Institut für Physikalische Chemie, Universität Freiburg, Albertstrasse 23a, D-79104 Freiburg, Germany

Received April 29, 2003; Revised Manuscript Received November 13, 2003

ABSTRACT: We focus on Vicsek fractals (VF), which are regular hyperbranched macromolecules. As such, they belong to the same family as the dendrimers, without suffering from the growth problems of the latter. We compute the mechanical and dielectric properties of VF in dilute solutions. The evaluation of the static and dynamical properties of VF in the framework of generalized Gaussian structures (GGS) reveals that they, distinct from the dendrimers, obey scaling. Theoretically speaking, VF are probably the most natural extension of GGS from linear chains to nontrivial loopless fractal objects. We encourage the synthesis and experimental characterization of the properties of this class of hyperbranched macromolecules.

1. Introduction

A fundamental problem in the study of polymers is in how far the geometrical properties of the macromolecules are reflected by their dynamical behavior. Historically, one proceeded from the fundamental theoretical investigations of dilute solutions of linear chains, pioneered by Rouse[1] and Zimm,[2] progressing from star polymers[3] and dendrimers[4−7] to more general hyperbranched structures[8−10] and to very complex macromolecular systems.[11−14] Now, the quest to model the dynamics of general polymer structures and that of their segments leads to the extension of the Rouse and Zimm approaches[1,2,15,16] to generalized Gaussian structures[17] (GGS): These consist of beads subject to friction (with friction constant ζ) connected to each other by springs (with elasticity constant K). The geometry is then taken into account by connecting each bead of the system to its nearest neighbors (which can be more than two). A central, simplifying assumption is that the connecting springs behave harmonically, so that the whole structure obeys Gaussian statistics. Additionally one can take hydrodynamic interactions (HI) into account, e.g., following Zimm, by using the preaveraged Oseen tensor.[2,15,16]

Now, the price to be paid in going from linear chains to star polymers,[18,19] dendrimers,[9,18−20] and general hyperbranched structures[21] is that scaling (at least in its classical form) is not expected to hold anymore (at least not in a simple form, which implies power-law dependences on the frequency ω or on the time t). The basic reason for this resides in the fact that while linear chains are (admittedly, trivial) fractals, the more general structures described above are not necessarily fractal.

Interestingly there exists a family of hyperbranched structures which obey dilation symmetry, the so-called Vicsek fractals (VF). VF can be constructed iteratively, by going from generation g to generation $g + 1$ in a deterministic way (which reminds one of the construction of dendrimers). The original VF with coordination number $f = 4$ were introduced in the 1980s[22] and their dynamical properties were investigated at the beginning of the 1990s.[23−26] From this work, it became clear that the eigenfunctions of VF, and in particular their eigenvalues, obey rather simple rules; the authors of refs 23−26 computed the eigenvalues of VF with $f = 4$, by determining numerically the roots of iteratively constructed polynomials.

In this work, we will point out that one can envisage (for different f values) the synthesis of macromolecules in VF form; this prompts us to analyze theoretically the properties of general VF. Furthermore, as we proceed to show, for arbitrary f and g the VF eigenvalues can be determined exactly, using simple algebraic recurence formulas. In this way the theoretical study of the dynamical properties of general VF is considerably simplified. This is particularly important, since in the framework of Rouse GGS models, many dynamical properties of easy experimental access are determined by the eigenvalues only. Moreover, VF are of much theoretical interest, since they are nontrivial fractals devoid of loops; in fact they may even be viewed (paralleling the dendrimers) as being another natural generalization of linear chains to regular branched structures with model character.

In previous work, we have shown how to deal with regular Sierpinski-type lattices using GGS procedures; in the Rouse variant, these allow one to determine the eigenvalues of macroscopically large objects to extremely high accuracy, without the need to diagonalize the connectivity matrices.[27,28] In this way, we could demonstrate that the main parameter that determines the Rouse dynamics is the spectral dimension of the fractals considered.[29−33] We could also show that for the Rouse-model scaling is very well obeyed over wide ranges in frequency or time, provided that the finite fractals considered are large enough.[27,28] Similar procedures can now be utilized in the study of VF, as we proceed to show.

The paper is structured as follows: In the next section, we introduce the VF for arbitrary f values and sketch a possible reaction scheme for synthesizing such VF. We also display a method which allows us to obtain exactly, in quite straightforward fashion, for arbitrary

[†] Theoretische Polymerphysik, Universität Freiburg.
[‡] Institut für Physikalische Chemie, Universität Freiburg.

10.1021/ma034553g CCC: $27.50
Published on Web 12/24/2003

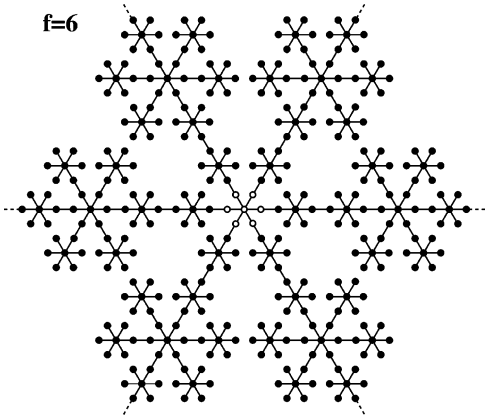

Figure 1. Vicsek fractal for $f = 6$ at the stage $N = 7^3$, i.e., at generation $g = 3$. Displayed is an absolutely regular realization, very atypical for the GGS's configuration in solution.

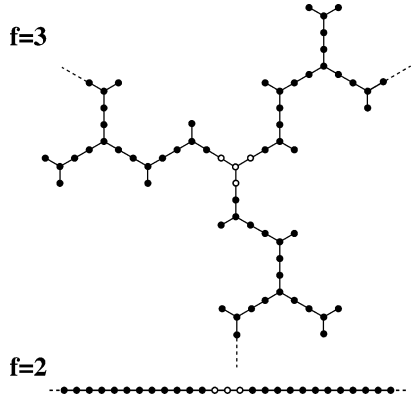

Figure 2. Vicsek fractals at generation $g = 3$ for $f = 3$ and $f = 2$. See also Figure 1 for comments.

f and g, all eigenvalues corresponding to a given finite VF. In section 3, we recall the general formalism of GGS which, in the Rouse picture, allows one to determine the dynamical properties of macromolecules in dilute solution based mainly on the eigenvalues of their connectivity matrices. In section 4 we calculate the mechanical and dielectric relaxation properties of VF, while also recalling the possibility of micromanipulating them; for this we evaluate the (anomalous) drift behavior of VF under the influence of external fields. Here we also prove that for VF all these dynamical features obey scaling. In section 5, we display the changes that occur when, in the spirit of Zimm, hydrodynamic interactions (HI) are also included in the picture. We conclude with a summary of results in section 6.

2. Generalized Vicsek Fractals

We now turn to a class of hyperbranched polymers which are connected in the form of VF. Our study is motivated by the search of scaling;[33,34] as we will demonstrate, such regular hyperbranched structures[23−26,35] obey scaling.

To render the iterative procedure clear we begin with a VF with functionality $f = 6$. In Figure 1, we show schematically the structure at generation $g = 3$. In the figure, the VF at generation $g = 1$ is represented through open circles; it consists of $f + 1 = 7$ beads arranged in a star-wise pattern, the central bead having six neighbors. To this object, one attaches at the next generation through 6 (in general f) bonds, again in star-wise fashion 6 (in general f) identical copies of itself. Hence, the next stage object ($g = 2$) consists of Figure 1 of 49 beads. The iteration is now obvious; Figure 1 presents the finite VF for $f = 6$ and $g = 3$. Note that the regular pattern of Figure 1 (embedded in the 2d-Euclidean space) has a fractal dimension $\bar{d}_r$ of

$$\bar{d}_r = \frac{\ln(f+1)}{\ln 3} \tag{1}$$

since increasing from the center the distance (radius) by a factor of 3 increases the number of beads inside it by $(f + 1)$. It differs from the $\bar{d}_f$ fractal dimension corresponding to the mass of the dendrimer in solution by a factor of 2, so that $\bar{d}_f = 2\bar{d}_r$. One should remark, as is also clear from eq 1, that the extreme overcrowding found for dendrimers (where $\bar{d}_r = \infty$) does not appear in VF. As examples for other members of the class, we depict in Figure 2 the VF for $f = 3$ and $g = 3$, as well as for $f = 2$ and $g = 3$. Note that the latter is, in fact, a linear chain.

We stop to remark that many dynamical properties of connected structures (such as the vibrational spectra, the relaxation modes, but also random walks over them) depend on the spectrum of the eigenvalues of their connectivity matrix $\mathbf{A} = (A_{ij})$. In this matrix the off-diagonal elements A_{ij} are -1 if beads i and j are connected by a bond, and 0, otherwise; furthermore the A_{ii} obey $A_{ii} = -\sum_{j\neq i} A_{ij}$. Previous work[23−26,35] has centered on finite VF with functionality $f = 4$; for this case, Jayanthi and Wu[24−26] succeeded in determining the eigenvalues of $\mathbf{A}$ by numerically computing the zeros of iteratively determined polynomials. Here we re-analyze the problem for general f and show that the eigenvalues of VF can be obtained in a straightforward way, for arbitrary f and g, through an algebraic iterative procedure, which involves the Cardano-solution for cubic equations.[36] These findings open the way to theoretically study the dynamics of arbitrarily large, finite VF.

Let us now first discuss some aspects related to the chemical realization of VF. These include the geometry in terms of composition, structure and steric requirements and the synthesis of the system. As is evident from Figures 1 and 2, VF are built from structural entities with valence c, which equal 1, 2 and f, entities which we denote by M_1, M_2, and M_f, respectively. Note that the case $f = 2$, in which only M_1 and M_2 appear, is particular, and that it leads to linear chains.

Considering the chemical aspects, one may first start with entities which are identical; however, if the macromolecules should extend to length scales considerably larger than those of the chemical bonds themselves, M_1, M_2, and M_f may also be chosen from a set of different chemical species. One has then a large variety of M_f entities at one's disposal, such as the building blocks of polycarbosilanes[37] or copolyester;[38] moreover, numerous other examples for M_f may be found. For $f = 3$, condensed triarylamines are interesting candidates; they have been synthesized as bridged molecules[39] and exist in a polymer phase.[40] A structural representation of this class of systems is given in Figure 3 for $g = 2$. Here the structural units are nitrogen atoms (M_3) and phenyl rings (M_1, M_2); for M_2 they are then connected in the para position. We note that even the connectivity $f = 6$ can be met by using triarylamines bound to rather small benzene rings.[41]

Although the thus created objects do not suffer from the extreme overcrowding of dendrimers, embedding

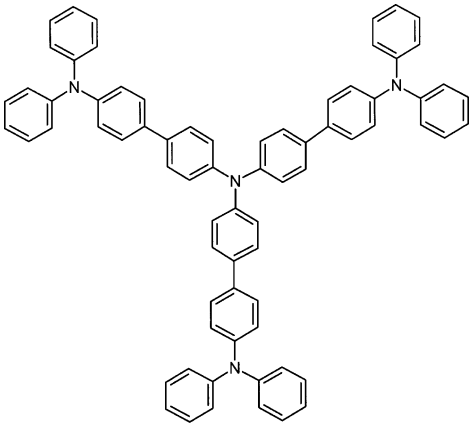

Figure 3. Suggested chemical realization of a Vicsek fractal with $f = 3$ at generation $g = 2$.

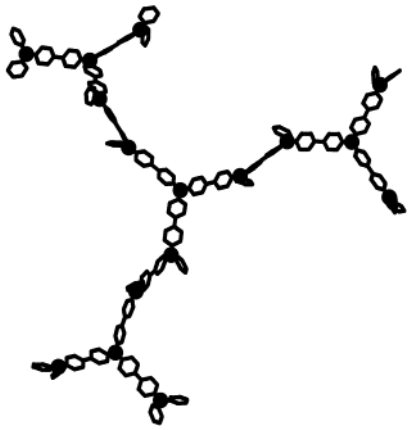

Figure 4. Two-dimensional display of an optimized three-dimensional model of a chemical realization of the Vicsek fractal with $f = 3$ at generation $g = 2$. The nitrogen atoms are represented as spheres; for convenience, the hydrogen atoms are not shown.

chemical realizations of Vicsek fractals with a high connectivity, i.e., $f \geq 5$, into three Euclidian dimensions may lead to serious packing problems and strong steric requirements, see $\bar{d}_f$ given after eq 1. In such cases, one has to take particular care while using the Gaussian model, and correlations may play an important role. In the chemical example of condensed triarylamines presented here, however, we have $f = 3$, which leads to $\bar{d}_f \simeq 2.52$, which is well below $d = 3$. To verify that the realization of the fractal is well-embedded in three dimensions, we have constructed models for the generations $g = 2$, 3, and 4 and relaxed them using a classical force field.[42] As is evident from Figure 4, the spatial requirements can be met without problems for systems that exhibit two-coordinated bridging elements that are not extremely bulky.

We continue by giving an outline of possible synthetic routes for the chemical realizations of VF. As we aim to obtain rather large structures, the reactions involved in the synthesis should be simple and allow for repetition in each generation. We now take the global reaction to be of the type given in Figure 5 and assume the A and B to be groups that react completely, e.g., within a condensation reaction; this comprises the first step of the scheme

$$M_4A_3 + 3M_4BC \rightarrow M_{16}C_3 + 3AB \qquad (2)$$

whereas the group C is not reactive in this step. We note

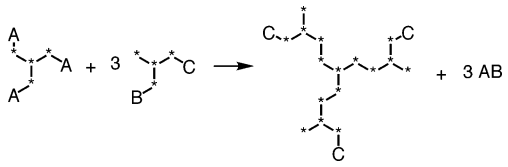

Figure 5. Condensation reaction within the synthesis of chemical realizations of Vicsek fractals.

that A and B do not necessarily have to be eliminated from the product molecule; they may even participate in a chemical bond that is stable with respect to the following reaction steps. In reaction 2, M constitutes the monomer, and it is indicated by the stars in the structure formula shown in Figure 5. The product of reaction 2 is divided into two fractions. For the first fraction, C is completely substituted by A

$$M_{16}C_3 \xrightarrow[+\,A]{-\,C} M_{16}A_3 \qquad (3)$$

In the second fraction, C is partly substituted by B, followed by an incomplete removal of the remaining C groups

$$M_{16}C_3 \xrightarrow[+\,B]{-\,C} M_{16}B_nC_m \qquad (4)$$

with m and n being 0, 1, 2, or 3 each. Consequently, a mixture of products $M_{16}B_nC_m$ is obtained, which has to be separated. This separation is unavoidable, because in the following step

$$M_{16}A_3 + 3M_{16}BC \rightarrow M_{64}C_3 + 3AB \qquad (5)$$

the next generation of the fractal has to be synthesized, whereby one has to avoid situations such as additional condensations ($n > 1$), having no reaction at all ($n = 0$), or having the reaction end for one branch in the next generation ($m > 1$). The B and C groups and the reaction conditions should be chosen in such a way as to give the maximum yield of $M_{16}BC$ in a mixture of 10 possible products (we consider $n \geq m$). In addition, B and C should differ in their properties, e.g., in ionicity, so that to enable a ready separation, i.e., by chromatography. We close by noting that the proposed scheme (eqs 2−5) sketches only a possible synthetic route and that the details require the skill and the experience of organic chemists in finding appropriate A, B, C, and M reactants, given that the basic steps of the scheme must occur at high yield.

After sketching a possible synthesis of macromolecules with VF geometry, we return to the determination of the eigenvalues of the VF. For this we derive recurrence formulas which allow us to obtain the eigenvalues of the $g + 1$ generation from that of the g generation. From these quantities, we determine for the corresponding VF the mechanical storage moduli, the dielectric relaxation forms and also the average displacements of the VF monomers under constant forces as a function of time. As we will show, in a Rouse framework these quantities scale, with exponents which depend only on the spectral dimension $\bar{d}$ of the corresponding VF.

The determination of the eigenvalues, i.e., the solution of

$$(\mathbf{A} - \lambda\mathbf{I})\mathbf{\Phi} = 0 \qquad (6)$$

starts from the facts pointed out above, namely that the

structure of a VF consists of three types of vertexes (entities, beads): f-coordinated centers (fCC, the M_f), beads on connecting bonds (the M_2), and also beads at the ends of dangling bonds (the M_1); hence each of the beads of a VF has either f, 2, or 1 neighbors. In the following, we inspect the eigenvalue problem, eq 6, and denote the components of the eigenvector $\mathbf{\Phi}$ by ϕ_j. Setting ϕ_0 for a particular fCC component in eq 6, the equation corresponding to the row containing this component as a diagonal element reads

$$(f - \lambda)\phi_0 = \sum_{j=1}^{f} \phi_j \tag{7}$$

where the ϕ_js are the eigenvector components corresponding to the topological neighbors of the fCC; these may themselves be either singly or doubly coordinated. The corresponding equations characteristic for sites with two neighbors are

$$(2 - \lambda)\phi_j = \phi_0 + \phi_m \tag{8}$$

where ϕ_0 is the eigenvector component of the fCC that is a neighbor of j, and ϕ_m denotes the component of the two-coordinated neighbor of j. Finally, for a dangling-bond component ϕ_1 we obtain in a similar way

$$(1 - \lambda)\phi_1 = \phi_0 \tag{9}$$

One can now transform, by simple algebraic means, all such equations to a set involving the coordinates of nearest-neighboring fCC only; by this the beads with coordination numbers 2 and 1 get suppressed. The details are given in the Appendix. The result is that in the new, decimated lattice eqs 7−9 get replaced by (see eqs 79, 72, and 60 of the Appendix)

$$[f - P(\lambda)]\tilde{\phi}_0 = \sum_{j=1}^{f} \tilde{\phi}_j \tag{10}$$

$$[2 - P(\lambda)]\tilde{\phi}_f = \tilde{\phi}_0 + \tilde{\phi}_m \tag{11}$$

and

$$[1 - P(\lambda)]\tilde{\phi}_1 = \tilde{\phi}_0 \tag{12}$$

in which we set

$$P(\lambda) = \lambda(\lambda - 3)(\lambda - f - 1) \tag{13}$$

In this way eqs 10−12 reproduce basically eqs 7−9. This, in fact, allows one to iterate at will the decimation procedure outlined above; then starting with $p_1(\lambda) = P(\lambda)$, in the kth iteration $P(\lambda)$ gets replaced by $p_k(\lambda) = P(p_{k-1}(\lambda))$. For finite VF this also allows (apart from the eigenvalue $\lambda_1 = 0$, which is special) to determine the eigenvalues at generation $g + 1$ from those at generation g through the relation

$$P(\lambda_i^{(g+1)}) = \lambda_i^{(g)} \tag{14}$$

Note that in this way each previous eigenvalue $\lambda_i^{(g)} \neq 0$ gives rise to three new ones (this fact, but not the following method, was already remarked upon in refs 23, 24, 25, 26, and 35 for the case $f = 4$). We can namely start from eqs 10−14 and compute the $\lambda_i^{(g)}$ iteratively, given that the roots of the polynomial

$$P(x) - a = x^3 - (f + 4)x^2 + 3(f + 1)x - a = 0 \tag{15}$$

are readily determined by introducing

$$p = \frac{1}{3}[f(f - 1) + 7] \tag{16}$$

$$q = \frac{1}{27}(5 - f)(f + 4)(2f - 1) \tag{17}$$

and

$$\rho = |p/3|^{3/2} \tag{18}$$

since then the roots of eq 15 are given by the Cardano solution; see ref 36

$$x_\nu = (f + 4)/3 + 2\rho^{1/3} \cos((\phi + 2\pi\nu)/3) \tag{19}$$

with $\nu \epsilon \{1, 2, 3\}$, where

$$\phi = \arccos((a - q)/2\rho) \tag{20}$$

Evidently then, one can identify in eq 15 the constant a with $\lambda_i^{(g)}$, from which, with eq 19, three new eigenvalues $\lambda_i^{(g+1)}$ of the next generation follow. This procedure makes also clear that the new eigenvalues keep the degeneracy of their predecessors.

To be able to determine the eigenvalues in a systematic way, it is very important to focus on the underlying eigenmodes. Following the procedure of Jayanthi and Wu[24−26] for $f = 4$, we find also for general f that the spectrum of VF is composed of nondegenerate and of degenerate eigenvalues. Fundamental for the nondegenerate modes is that they always involve a moving central bead. Modes belonging to degenerate eigenvalues, on the other hand, are characterized by the fact that the central bead does not move.

We now proceed to show that in this way we obtain all eigenvalues. First, at every generation the nondegenerate mode $\lambda_1 = 0$, is always present; furthermore there is one nondegenerate mode corresponding to the eigenvalue $(f + 1)$ and there are Δ_g degenerate modes corresponding to the eigenvalue 1; these are characterized by the fact that in them all fCC are immobile. Following the argument of ref 26, one may determine Δ_g and create these modes iteratively, by going from generation $g - 1$ to g. Then, given that in the construction $(f + 1)$ VF of generation $g - 1$ get attached to each other by f bonds, one has to observe f constraints. The degrees of degeneracy are hence related through

$$\Delta_g = (f + 1)\Delta_{g-1} - f \tag{21}$$

For $g \geq 1$, the Δ_g fulfill then (see also the Appendix for another derivation):

$$\Delta_g = (f - 2)(f + 1)^{g-1} + 1 \tag{22}$$

Moreover, eigenvalues which appeared at one generation continue to appear in all subsequent generations (they are called "persistent"[24−26]). As noted above, apart from $\lambda_1 = 0$, each of the other eigenvalues (degenerate or nondegenerate) at generation g, e.g., $\lambda_i^{(g)}$, produces three new, different eigenvalues (e.g., $\lambda_{i1}^{(g+1)}$, $\lambda_{i2}^{(g+1)}$, and $\lambda_{i3}^{(g+1)}$) at generation $g + 1$.

We now prove that this procedure gives at generation g a total of $N = (f + 1)^g$ eigenvalues, total which corresponds exactly to the number of beads in the system. Here, one should first remember that each bead (vertex) provides only one component to eq 6, i.e., one has exactly one degree of freedom per bead. Furthermore, in the GGS scheme discussed in the next Section (as is usual for Rouse-type models) the three position components of each bead decouple, so that it is again sufficient to consider only one component for each bead. Turning now tho the evaluation of the number of nondegenerate modes $N_g^{(\mathrm{nd})}$ at generation g one has

$$N_g^{(\mathrm{nd})} = 1 + 1 + 3 + ... + 3^{g-1} = 1 + \sum_{i=0}^{g-1} 3^i = 1 + (3^g - 1)/2 \quad (23)$$

where we took into account the $\lambda_1 = 0$ mode and remembered that each additional mode gives rise to 3 modes in the next generation and hence to 3^2 modes in the following one, etc. On the other hand, in each generation j, an additional number of Δ_j eigenvalues to $\lambda = 1$ appear, a degeneracy which their offspring keeps. Hence the number $N_g^{(\mathrm{d})}$ of degenerate modes at generation g is

$$N_g^{(\mathrm{d})} = \Delta_g 3^0 + ... + \Delta_1 3^{g-1} = \sum_{i=0}^{g-1} \Delta_{g-i} 3^i \quad (24)$$

which, with Δ_g given by eq 22, reads

$$N_g^{(\mathrm{d})} = \sum_{i=0}^{g-1} 3^i + (f-2)(f+1)^{g-1} \sum_{i=0}^{g-1} 3^i/(f+1)^i = (3^g - 1)/2 + [(f+1)^g - 3^g] \quad (25)$$

Hence, as claimed above

$$N_g^{(\mathrm{nd})} + N_g^{(\mathrm{d})} = (f+1)^g \equiv N \quad (26)$$

Focusing on the spectral region of small λ now allows one to determine the so-called spectral dimension $\tilde{d}$ of the VF. The starting point is the observation that for small λ one can linearize eq 15 and obtain as an iteration scheme from eq 14

$$3(f+1)\lambda_i^{(g+1)} = \lambda_i^{(g)} \quad (27)$$

Numerically, one finds that repeated iterations lead to a stable spectrum. On the other hand, under eq 27, the M eigenvalues in the interval $[\lambda^{(g)}, \lambda^{(g)} + \Delta\lambda]$ go over in M eigenvalues in the interval $[\lambda^{(g+1)}, \lambda^{(g+1)} + \Delta\lambda/(3f + 3)]$. At the same time, the total number of modes increases from N to $(f + 1)N$. This means that the density of modes for small λ obeys

$$\rho(\lambda)\Delta\lambda = (3f+3)\rho(\lambda/(3f+3))\Delta\lambda/(f+1) \quad (28)$$

$$\text{i.e.,} \quad \rho(\lambda) = 3g(\lambda/(3f+3)) \quad (29)$$

This implies a power-law relation, which reads in the usual notation

$$\rho(\lambda) \sim \lambda^{\tilde{d}/2-1} \quad (30)$$

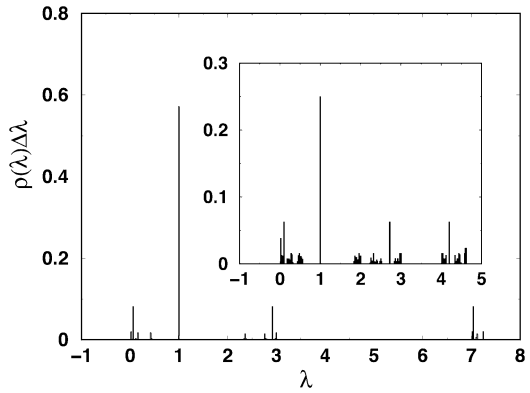

Figure 6. Density of states $\rho(\lambda)\Delta\lambda$ for VF with $g = 13$. The main figure gives the case $f = 6$, hence $N = 7^{13}$, the insert the case $f = 3$, hence $N = 4^{13}$. The width of the bins is in both cases $\Delta\lambda = 0.02$.

It follows by inserting eq 30 into 29 that

$$1 = 3[3(f+1)]^{\tilde{d}/2-1} \quad (31)$$

from which one obtains $\tilde{d}$ for general VF:

$$\tilde{d} = \frac{2\ln(f+1)}{\ln(3f+3)} \quad (32)$$

This is the generalization for arbitrary f of the previously obtained result[26,35] for $f = 4$.

We used the above procedure, eqs 19 and 20, and determined exemplarily, for $f = 2$, 3, 4, and 6 the eigenvalues of Vicsek fractals, recovering, for $f = 4$, all former findings.[23−26,35] For instance, for $f = 6$, we readily obtain the eigenvalues for fractals with N up to $N = 7^{13}$. For small VF, it is also possible to fully diagonalize the corresponding **A** matrices and to verify the correctness of the procedure (eigenvalues and degeneracies). For larger systems, e.g., for $f = 3$ and N up to $N = 4^8$, we have used the fact that the **A** matrices are sparse, and computed their eigenvalues based on a modified Lanczos algorithm.[74−76] The agreement is perfect. Note, however, that in its standard form, the Lanczos procedure then supplies only the eigenvalues, but not their degeneracy. For even larger systems, one reaches quite soon the limits of today's feasible numerical diagonalizations, while our iterative procedure is only limited by the number of digits employed.

We now consider the spectra which we obtained iteratively and display in Figure 6 as a histogram, for the Vicsek fractal with $f = 6$ and $g = 13$, i.e., for $N = 7^{13}$, the number of eigenvalues in intervals of width $\Delta\lambda = 0.02$. Furthermore, we present in the insert of Figure 6 the corresponding histogram for VF with $f = 3$ and $g = 13$, i.e., $N = 4^{13}$. Particularly striking are for both VF the discrete form of the spectra, the multitude of forbidden bands, and the inherent symmetries. Note that the forbidden bands are larger for the VF with $f = 6$ than for the VF with $f = 3$. As for dual Sierpinski gaskets[27,28] and paralleling earlier results[25,26,35,43,44] we find that the spectra consist of both a Cantor set and also of finite series of eigenvalues, the latter corresponding to localized modes. Nonetheless, as we will show, these spectra give rise to rather smooth mechanical and dielectric relaxation forms where, as is to be expected from Figure 6, the curves for VF with $f = 3$ will turn out to be smoother than those for the $f = 6$ case.

3. Generalized Gaussian Structures and Relaxation

In this section, we study the dynamics of VF in the framwork of the GGS. Given that the procedure was recently explained in detail,[17,18,32] we mainly summarize the basic results of the GGS formalism which we will use in the following. Now, the configuration of a GGS is given by a set of vectors $\{\mathbf{R}_k\}$, where $\mathbf{R}_k(t) = (R_{xk}(t), R_{yk}(t), R_{zk}(t)) = (X_k(t), Y_k(t), Z_k(t))$ is the position vector of the kth bead at time t. The GGS assumption is that the potential energy $U(\{\mathbf{R}_k\})$ is built only of harmonic terms, involving monomers directly bound to each other; including also interactions with external forces $\{\mathbf{F}_n\}$ the energy $U(\{\mathbf{R}_k\})$ reads

$$U(\{\boldsymbol{R}_k\}) = \frac{K}{2}\sum_{\beta,m,n} R_{\beta m}A_{mn}R_{\beta n} - \sum_{\beta,n} F_{\beta n}R_{\beta n} \qquad (33)$$

On the right-hand-side (rhs) of eq 33 β runs over the components x, y and z, and the GGS is taken into account through the $N \times N$ matrix $\mathbf{A} = (A_{mn})$. Following Kirkwood and Riseman[45] and Zimm[2] the hydrodynamic couplings between the beads may also be taken into account; one introduces the HI tensor, $\mathbf{H} = (H_{ij})$,whose components in the preaveraged picture are[6,15,46]

$$H_{ij} = (\delta_{ij} + \zeta_r\langle l/R_{ij}\rangle(1 - \delta_{ij})) \qquad (34)$$

Here $R_{ij} = |\mathbf{R}_{ij}| = |\mathbf{R}_i - \mathbf{R}_j|$ is the distance between beads i and j. The interbead distances are taken to be Gaussian distributed, so that

$$\langle R_{ij}^{-1}\rangle = \left(\frac{6}{\pi\langle R_{ij}^2\rangle}\right)^{1/2} \qquad (35)$$

In eq 34, $\zeta_r = \zeta/6\pi\eta_0 l$, where ζ is the friction coefficient, η_0 the solvent's viscosity, and l the average length of an isolated bond. Furthermore, the beads are subject to fluctuating forces, $\mathbf{f}_i(t)$, which are zero-centered and Gaussian distributed.

It is now a relatively straightforward matter to compute the dynamical properties, since the GGS problem is linear and the different components (X_i, Y_i, and Z_i) decouple. When $\sigma = K/\zeta$, $\mathbf{Y} = (Y_1, \ldots Y_N)^T$, and $\mathbf{f}(t)$ and $\mathbf{F}(t)$ analogously are introduced, the corresponding Langevin equation has the form

$$\frac{\partial \mathbf{Y}(t)}{\partial t} + \sigma\mathbf{H}\mathbf{A}\mathbf{Y}(t) = \frac{1}{\zeta}\mathbf{H}(\mathbf{f}(t) + \mathbf{F}(t)) \qquad (36)$$

What is now needed is the transformation

$$\mathbf{Q}^{-1}\mathbf{H}\mathbf{A}\mathbf{Q} = \mathbf{\Lambda} \qquad (37)$$

$\mathbf{\Lambda}$ being a diagonal matrix with elements λ_i. The details of the procedure were explicitly reported in ref 20. Relevant here is that there always exists a matrix $\mathbf{Q}$ which fulfills eq 37. Moreover, for a completely connected structure and for a physically reasonable inclusion of the HI (i.e., not too large ζ_r) the inverse $\mathbf{H}^{-1}$ exists, and the matrix $\mathbf{HA}$ has only one vanishing eigenvalue which we, as before, denote by λ_1, the other eigenvalues being positive.[20]

We continue by recalling that the mechanical relaxation is described by the complex dynamic modulus $G^*(\omega)$ or, equivalently, by its real $G'(\omega)$ and imaginary $G''(\omega)$ components (the storage and the loss moduli[47,48]), which for $\omega > 0$ and Rouse-type models read (see also eqs 4.159 and 4.160 of ref 15)

$$G'(\omega) = C\frac{1}{N}\sum_{i=2}^{N}\frac{(\omega/2\sigma\lambda_i)^2}{1 + (\omega/2\sigma\lambda_i)^2} \qquad (38)$$

and

$$G''(\omega) = C\frac{1}{N}\sum_{i=2}^{N}\frac{\omega/2\sigma\lambda_i}{1 + (\omega/2\sigma\lambda_i)^2} \qquad (39)$$

For very dilute solutions one has $C = \nu k_B T$, where ν is the number of polymer segments (beads) per unit volume; for concentrated solutions, when the entanglement effects are negligible, eqs 38 and 39 still hold, and only the value of C changes.[48,49] In eqs 38 and 39, the λ_i are the eigenvalues discussed above. Note that the factor 2 in the expressions $\omega/2\sigma\lambda_i$ arises from the second moment of the displacements involved in computing the stress required in the evaluation of $G^*(\omega)$.[15]

We now turn to consider dielectric relaxation expressions and note that their evaluation is based on the frequency-dependent, complex dielectric susceptibility, $\epsilon^*(\omega)$. Now one focuses usually on

$$\Delta\epsilon^*(\omega) = \frac{\epsilon^*(\omega) - \epsilon_\infty}{\epsilon_0 - \epsilon_\infty} \qquad (40)$$

where ϵ_0 and ϵ_∞ denote the limiting low- and high-frequency dielectric constants, respectively. In general, subjecting polar molecules embedded in nonpolar solvents to an alternating electric field $E = E_0 \exp(i\omega t)$ leads to the $\Delta\epsilon^*(\omega)$ response[50]

$$\Delta\epsilon^*(\omega) \simeq \int_0^\infty \left(-\frac{\mathrm{d}}{\mathrm{d}t}C_0(\mathbf{M}; t)\right)\exp(-i\omega t)\,\mathrm{d}t \qquad (41)$$

when the local fields are not important. In eq 41, the quantity $C_0(\mathbf{M}; t)$ is the normalized autocorrelation function of the total dipole moment $\mathbf{M}(t)$ of the system. Focusing now on the dielectric response of GGSs which possess dipole moments directed along their bonds (type A according to Stockmayer's classification),[51−53] one finds a straightforward correspondence between the mechanical and dielectric relaxation forms. One has namely[54]

$$\Delta\epsilon'(\omega) = 1 - G'(2\omega)/C \qquad (42)$$

and

$$\Delta\epsilon'' = G''(2\omega)/C \qquad (43)$$

One may furthermore note that the dielectric susceptibility, eqs 42 and 43, is determined by relaxation times which are twice larger[14] that those appearing in the expressions of the mechanical relaxation, eqs 38 and 39.

We now turn to the motion of individual monomers in external fields, an idealized case of micromanipulation experiments.[55−60] We let the external force start to act at $t = 0$ on one monomer contained in the GGS; then, we average over all possibilities of choosing this monomer randomly. The resulting (quenched) ensemble

averaged displacement reads[20]

$$\overline{Y(t)} \equiv \langle\langle Y(t)\rangle\rangle = \frac{F\tilde{H}_{1,1}t}{N\zeta} + \frac{F}{\sigma N\zeta}\sum_{i=2}^{N}\frac{1-\exp(-\sigma\lambda_i t)}{\lambda_i}\tilde{H}_{ii} \tag{44}$$

where $\tilde{H}_{ii} = \sum_{k,l} Q_{ik}^{-1}H_{kl}Q_{li}$, so that $\tilde{H}_{1,1}$ is simply $\tilde{H}_{1,1} = \sqrt{N}\sum_k Q_{1k}^{-1}H_{k1}$.

We remark that the final expression involves only the eigenvalues of the matrix **HA** and the $\tilde{H}_{ii}$. In eq 44, the translational motion associated with the *drift center* (DC) has separated from the rest; we recall that the DC is defined through[5,6]

$$\mathbf{R}_{\mathrm{DC}}(t) = \frac{\sum_{i,j}\mathbf{H}_{ij}^{-1}\mathbf{R}_j(t)}{\sum_{i,j}\mathbf{H}_{ij}^{-1}} \tag{45}$$

One may notice that in the Rouse case, where $\mathbf{H} = \mathbf{I}$, the DC is identical to the center-of-mass; in general, however, this does not hold. Moreover, for $\mathbf{H} = \mathbf{I}$, i.e., $H_{kl} = \delta_{kl}$, all $\tilde{H}_{ii}$ equal unity, and eq 44 depends only on the eigenvalues of **A**, but not on its eigenvectors; $\overline{Y(t)}$ simplifies then to

$$\overline{Y(t)} = \frac{Ft}{N\zeta} + \frac{F}{\sigma N\zeta}\sum_{i=2}^{N}\frac{1-\exp(-\sigma\lambda/t)}{\lambda_i} \tag{46}$$

From eq 44, the behavior of the motion for extremely short and for very long times is obvious: one has in the limit of very short times $\overline{Y(t)} = Ft/\zeta$, since $\mathrm{Tr}(\tilde{\mathbf{H}}) = \mathrm{Tr}(\mathbf{Q}^{-1}\mathbf{HQ}) = \mathrm{Tr}(\mathbf{H}) = N$, see eq 34. In the opposite limit, for very long times one has $\overline{Y(t)} = F\tilde{H}_{1,1}t/N\zeta$. The interpretation is that at very short times only one bead is moving, whereas at long times the whole GGS drifts. These very general features make clear that the particular structure of the GGS is revealed in the intermediate domain of times (or frequencies);[18,20,27,28,31−33] there, the behavior indeed depends in a detailed way on the eigenvalues and eigenvectors and thus on **A** and, depending on the model, also on **H**.

In the next section, we will consider what happens with structures modeled by finite VF in the Rouse scheme (i.e., $\mathbf{H} = \mathbf{I}$). Fractals are of fundamental importance as simply structured, highly nontrivial scaling objects.[17,29−33,61−68] Now, VF are special in that they (as the related dendrimers[5−8,19−21,69]) belong to the class of hyperbranched polymers.[3] In studying the VF dynamics, we will consider their mechanical and dielectric relaxation forms and also the motion of their monomers under external forces.

4. Rouse-Dynamics of Generalized Vicsek Fractals

As shown above, the relaxation forms eqs 38, 39, and 44, require the knowledge of the eigenvectors and eigenvalues of the matrices **A**, **HA**, and $\mathbf{Q}^{-1}\mathbf{HQ}$. In the absence of HI (Rouse case), it is sufficient to know all the eigenvalues of **A** in order to determine the global behavior of the system. In the presence of HI one needs first to diagonalize **A** in order to obtain, based on eqs 34 and 35, the matrix **H**; the diagonalization of **HA** leads then to the eigenvalues needed in eqs 38 and 39, whereas the diagonal elements of the matrix $\mathbf{Q}^{-1}\mathbf{HQ}$ are also required in order to compute $\overline{Y(t)}$ based on eq 44.

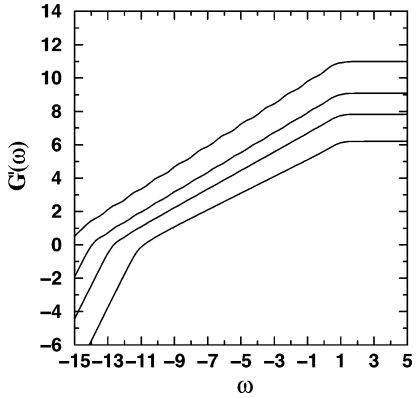

Figure 7. Normalized storage modulus $G'(\omega)$ for the Rouse model, shown in dimensionless units for $g = 13$ and $f = 2$, 3, 4, and 6 from below and hence for $N = 3^{13}$, 4^{13}, 5^{13}, and 7^{13}, evaluated according to eq 38. The scales are double logarithmic to basis 10.

We are now in the position to use the eigenvalues obtained in order to calculate in the Rouse case ($\mathbf{H} = \mathbf{I}$) the different relaxation forms discussed in section 3. We start by focusing on the mechanical relaxation modulus $G'(\omega)$, given by eq 38, which we present in double-logarithmic scales in Figure 7. Here we vary f and use VF with $g = 13$ and f equal to 2, 3, 4, and 6; hence, N goes from 3^{13} to 7^{13}. We plot eq 38 in dimensionless units, by setting $\sigma = 1$ and $C/N = 1$. Clearly evident from Figure 7 are the limiting, connectivity-independent behaviors at very small and very high ω; for $\omega \ll 1$ one has $G'(\omega) \sim \omega^2$ and for $\omega \gg 1$ one finds $G'(\omega) \sim \omega^0$. The fractal aspect is given by the between regions, where in the double-logarithmic scales of Figure 7 the $G'(\omega)$ appear as roughly straight lines, with slopes which increase with f. Furthermore, with increasing f there appears an increasing waviness of $G'(\omega)$. This is no inaccuracy of the calculations, but the sign of the underlying Cantor-set structure of the spectrum; for large f, the sum in eq 38 cannot smooth out this structure anymore, and the share of each generation gets to be visible in $G'(\omega)$. If we disregard this waviness, Figure 7 indicates that one has to a very good approximation

$$G'(\omega) \sim \omega^{\alpha'} \tag{47}$$

i.e., that $G'(\omega)$ scales in the intermediate domain. Now, a more detailed analysis[27−30] shows that in the limit $N \to \infty$ one should have $\alpha' = \tilde{d}/2$, where $\tilde{d}$ is the spectral dimension, eq 32. The data of Figure 7 support this very well; using a linear approximation in the scaling regime leads for $f = 2$, 3, 4, and 6 to $\alpha' = 0.504$, 0.557, 0.595, and 0.640, respectively, to be compared with the theoretical value $\tilde{d}/2 = \ln(f+1)/\ln(3f+3)$, namely to $^1/_2$, 0.55789, 0.59432, and 0.63975. This very good agreement is due to the fact that the N values used in Figure 7 are very large; we can attain them due to our method of calculation of the eigenvalues. We note that if N is rather small, e.g., around 1000, due to the substantial crossover domains, the slope which can be inferred from the moduli is rather far from $\tilde{d}/2$; to obtain this value accurately, larger GGS are needed. On the other hand, diagonalizing numerically (for other GGS families) matrices much larger than 5000 × 5000 is by no means

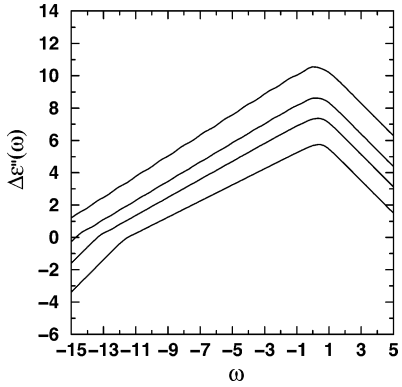

Figure 8. Normalized dielectric relaxation $\Delta\epsilon''(\omega)$ for the Rouse model, shown for the same N values as in Figure 7 and evaluated according to eq 43, see the text for details. The scales are as in Figure 7.

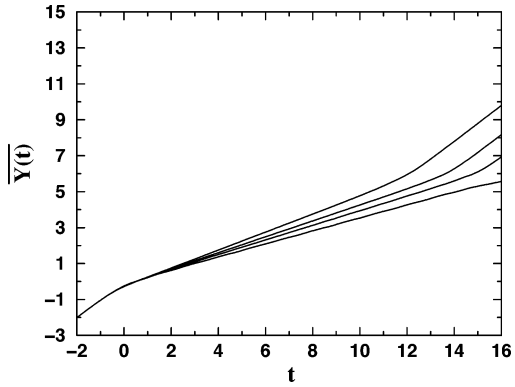

Figure 9. Averaged monomer displacement $\overline{Y(t)}$ under the action of an external force in the Rouse picture. Displayed are in double logarithmic scales to basis 10 and in dimensionless units the normalized $\overline{Y(t)}$ for $N = 3^{13}$, 4^{13}, 5^{13}, and 7^{13} from above, see the text for details.

trivial, requiring the diagonalization[70,71] and inversion[72] of nonsparse matrices.

Given that $G''(\omega)$ and $\Delta\epsilon''(\omega)$ are very similar, see eq 43, we choose to continue with the dielectric relaxation. For this we display $\Delta\epsilon''(\omega)$ in Figure 8 under the same conditions as $G'(\omega)$ of Figure 7. Now the limiting cases for small and large ω are $\Delta\epsilon''(\omega) \sim \omega$ and $\Delta\epsilon''(\omega) \sim \omega^{-1}$, respectively. Again concentrating on the intermediate domain, we find for $f = 2$, 3, 4, and 6 that the slope of $\Delta\epsilon''(\omega)$ in the double logarithmic scales of Figure 8 changes from 0.5, 0.556, 0.593 to 0.637. Again these values compare very favorably to the theoretically expected $\tilde{d}/2$, given above. As noted in previous works,[18−20,28,73] we find that the numerically determined slopes for $G''(\omega)$, i.e., for $\Delta\epsilon''(\omega)$, are systematically lower than those for $G'(\omega)$. Moreover, also from Figure 8, we remark that the waviness of the curves increases with larger f. Overall, however, we find that the spectral dimension gives a good picture of the scaling behavior in the Rouse case.

We finish by focusing in Figure 9 on the averaged monomer displacement $\overline{Y(t)}$ in the Rouse scheme; in eq 46, we set $\sigma = 1$ and $F/\zeta = 1$. The results are again presented in double-logarithmic scales for finite VF ranging from $N = 3^{13}$ to $N = 7^{13}$. Clearly evident from the figure is, for $f = 2$, 3, and 4, that at long times one reaches the domain $\overline{Y(t)} \sim Ft/(N\zeta)$, which, in the absence of an external field (based on the Einstein relation for GGS[20]), is the hallmark of simple diffusion.

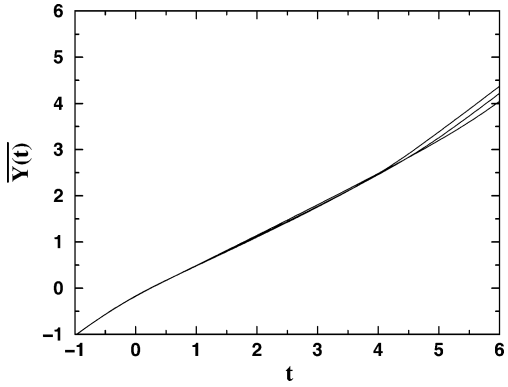

Figure 10. Averaged monomer displacement $\overline{Y(t)}$ of Vicsek fractals under the action of external forces in the Zimm model for $\zeta_r = 0.25$. Displayed are (on the rhs. from below) the results for $N = 4000$, 4096, and 3125 for $f = 2$, 3 and 4, respectively. The scales are as in Figure 9.

Because of this N dependence of $\overline{Y(t)}$, in Figure 9 at long times the curves belonging to VF of different f are shifted with respect to each other. Moreover, at very short times $\overline{Y(t)} \simeq Ft/\zeta$ for all N. Again, typical for the *fractal* structure is the intermediate regime. In the double logarithmic scales of Figure 9 this subdiffusive, scaling domain appears (as in Figure 3 of ref 27) as a straight line; it obeys

$$\overline{Y(t)} \sim t^{\gamma} \tag{48}$$

where theoretically one expects[27,28,31−33]

$$\gamma = 1 - \tilde{d}/2 \tag{49}$$

$\tilde{d}$ being again the spectral dimension.

Using the slopes of the curves of Figure 9 in the intermediate regime, we determine numerically the parameter γ of eq 48, and find for $f = 2$, 3, 4, and 6 that $\gamma = 0.501$, 0.442, 0.407, and 0.361, to be compared with $1 - \tilde{d}/2 = {}^1/_2$, 0.44211, 0.40568, and 0.36084, respectively. The accuracy attained is certainly sufficient to allow us to claim that for VF and for the dynamical forms analyzed here the sole fractal parameter of importance is indeed $\tilde{d}$. These VF results complement in a nice way similar findings for dual Sierpinski gaskets.[27,28]

Summarizing, in the Rouse GGS model, we find that for VF the mechanical and dielectric relaxation forms scale and that the scaling exponents are well-represented by simply taking only the VF spectral dimension into account. Moreover, scaling is also evident in the subdiffusive drift motion of the VF and in the average motion of monomers under external forces. We now turn to the evaluation of these dynamical quantities in the presence of HI.

5. Zimm-Dynamics of Vicsek Fractals

We are now in the position to use the theory developed in section 3 in order to calculate numerically the different relaxation quantities for Vicsek fractals under HI. We prefer to start from the averaged monomer displacement $\overline{Y(t)}$, eq 44, in which we set $\sigma = 1$ and $F/\zeta = 1$ and present in Figure 10 the HI results for finite VF with $f = 2$, 3, and 4, and for $\zeta_r = 0.25$. We have taken the N values to be $N = 4000$ for $f = 2$, $N = 4^6 = 4096$ for $f = 3$, and $N = 5^5 = 3125$ for $f = 4$. Evidently, given

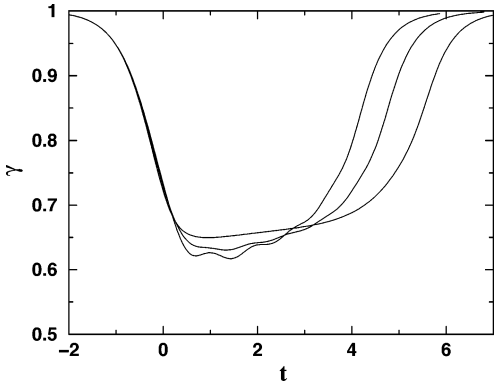

Figure 11. Slopes $\gamma = d(\log_{10} \overline{Y(t)})/d(\log_{10} t)$ of the averaged monomer displacement of VF under the action of external forces, plotted as a function of $\log_{10} t$. Displayed are the results of the Zimm model ($\zeta_r = 0.25$), for the VF given in Figure 10.

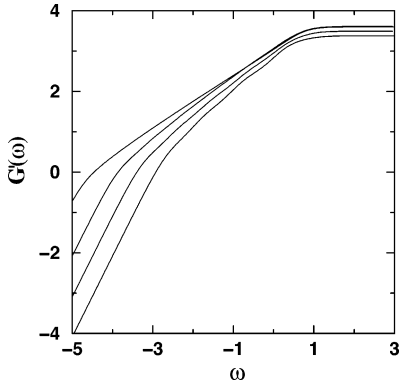

Figure 12. Normalized storage moduli $G'(\omega)$ for the Zimm model ($\zeta_r = 0.25$), shown in dimensionless units from above for $N = 4000$, 4096, 3125, and 2401 for $f = 2$, 3, 4 and 6, respectively. They were evaluated according to eq 38; see the text for details. The scales are as in Figure 7.

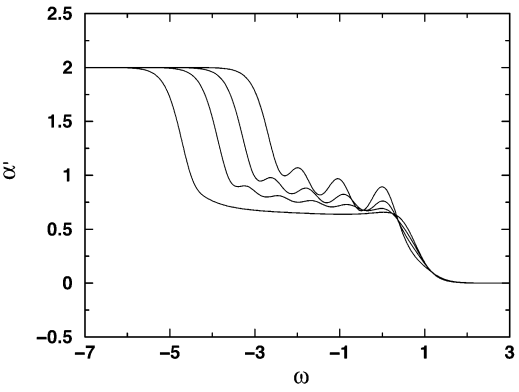

Figure 13. Effective slopes α′ of $G'(\omega)$ of Figure 12, plotted as a function of $\log_{10} \omega$, see the text for details.

that now we have to determine the eigenvalues through advanced diagonalization routines,[70−72] the attainable values for N are much more restricted than in the Rouse case. As before, for very short times all of the curves merge; this is the domain where $\overline{Y(t)} = Ft/\zeta$. Furthermore, at long times one reaches the domain $\overline{Y(t)} \simeq F\tilde{H}_{11}t/(N\zeta)$. In the logarithmic scales of Figure 10, these two domains appear as straight lines with slope 1. In all VF cases considered, under HI the intermediate range gets smaller (as was also established by us for other macromolecules in previous works[19,20]). Interestingly, the curves shown in Figure 10 also indicate the possibility of scaling; qualitatively, we find that in the intermediate regime one can well approximate the curves by straight lines, whose slopes are 0.66 for $f = 2$, 0.64 for $f = 3$, and 0.63 for $f = 4$. We also note that, in contrast to Figure 9, in Figure 10 the slopes of the curves in the intermediate regime hardly differ from each other; evidently, the dynamics of macromolecules under HI occurs as if the moving objects were more compact, and hence their internal dynamics does not show up so clearly as in the Rouse case. We note that the case $f = 2$ is the classical Zimm result for the linear chain. Indeed, as shown in ref 73, scaling is well obeyed for the linear chain under HI, with a power-law whose exponent is quite close to the value of $^2/_3$.

To display a more quantitative analysis of the dynamical data under HI, we plot in Figure 11 the quantity $\gamma = d \log (\overline{Y(t)})/d \log_{10}(t)$ as a function of $\log_{10} t$ for the VF of Figure 10. In this way one can see rather clearly for each f the appearance of a plateaulike regime at the approximate values of 0.66, 0.63, and 0.62 for $f = 2$, 3 and 4, respectively. Furthermore, some oscillations are evident; they are due to the internal structure of the VF and their hierarchical construction.

We now turn to the study of the mechanical relaxation and focus on the storage modulus $G'(\omega)$, which, paralleling Figure 7, we present in Figure 12. Here, we use VF with $f = 2$, 3, 4, and 6, with N being 4000, 4^6, 5^5, and $7^4 = 2401$, respectively. Plotted are the results of eq 38 for $\zeta_r = 0.25$, in dimensionless units, in which we set $\sigma = 1$ and $C/N = 1$. As in the Rouse case, Figure 7, again the limiting, connectivity-independent behaviors at very small and very high ω are evident; moreover, as before, the structure-dependent aspects are given by the intermediate regions. Now, as in former calculations[19,20] and as stressed in the discussion of Figure 10, the first clear-cut feature is that under HI the intermediate domain gets smaller. Now, where scaling is concerned, it appears that the slopes of $G'(\omega)$ vary somewhat as a function of ω.

To render these aspects more evident, we show in Figure 13 the quantity $\alpha' = \mathrm{d}(\log_{10} G'(\omega))/\mathrm{d}(\log_{10} \omega)$ for the VF of Figure 12; the α′ are in fact the derivatives of the curves (i.e., the slopes) displayed in Figure 12. Immediately apparent are for very small and for very large ω the limiting, theoretically expected values, namely 2 and 0; furthermore the intermediate domain shows clear transition regions. Note that the presentation in Figure 13 visually enhances the oscillations found in Figure 12; as the g dependence of the patterns makes clear, the oscillations are due to the hierachical construction of the VF.

For the intermediate domain, a theoretical effective medium approach was developed by Cates[29,30] for polymeric fractals; in this regime (called by him the high-frequency regime), his approach suggests a power-law scaling behavior for $G'(\omega)$. From these works,[29,30] under HI the exponent $\tilde{d}/2$ should get replaced by $\bar{d}_f/d$, see eqs 4.14 ff and 4.40 of ref 30, where $\bar{d}_f$ is the fractal dimension of the object in solution, $\bar{d}_f = 2\bar{d}_r$, with $\bar{d}_r$ being given by eq 1. This leads to the following theoretical estimate for the slopes:

$$\frac{\bar{d}_f}{d} = \frac{2 \ln(f+1)}{3 \ln 3} \tag{50}$$

Using eq 50, we obtain for $f = 2$, 3, 4, and 6 as theoretical values for the slopes 0.667, 0.841, 0.977, and 1.180, respectively. These values should be compared

to our numerical results, namely to $\alpha' = 0.66$ for $f = 2$, $\alpha' = 0.76$ for $f = 3$, $\alpha' = 0.81$ for $f = 4$, and $\alpha' = 0.88$ for $f = 6$. We thus find a discrepancy between the theoretically expected values and the numerical results; however, this discrepancy may be due to the fact that the VF used here in the Zimm case are by far smaller than those employed by us before in the Rouse case, where the agreement with the theoretical results turned out to be very good. This finding stresses again the importance to study very large systems and the advantage offered by our iterative scheme in determining the eigenvalues of **A** even for very large VF to high precision.

6. Conclusions

In this paper, we have concentrated on Vicsek fractals, a class of hyperbranched molecules whose dynamical properties obey scaling. After having sketched a possible chemical scheme for synthesizing macromolecules of VF character, we have demonstrated that these objects have well-determined fractal and spectral dimensions. Furthermore, as we have derived, the eigenvalues of the connectivity matrices of VF can be evaluated by iterative algebraic relations in a straightforward manner. In this way, we have also enlarged the theoretical knowledge about VF, given that up to now the literature focused on VF with coordination number $f = 4$. On the basis of eq 1, we remark that only coordination numbers $f \leq 5$ give rise to fractal dimensions that are smaller than the Euclidian dimension $d = 3$. In terms of f one thus has a natural limit for overcrowding. The VF cases $f = 3$ and $f = 4$ are, see eq 1, nonspace filling, and they can thus be extended to infinity (i.e., take g very large), regardless of the length of the connecting bonds. The cases $f \geq 5$ require more care, however, since a straightforward application of eqs 1 and 50 leads to having $d_m > 3$. But even then very large VF may be constructed by using relatively long chains as spacers. We are thus confident that such VF can be synthesized, possibly along the lines suggested by us, which involve triarylamines as building blocks.

Moreover, using our knowledge, we have calculated basic experimental quantities of the VF dynamics in solution, where we have also taken the influence of hydrodynamic interactions into account. The quantities considered were the mechanical and dielectric relaxation, as well as the stretching of the macromolecules under local external fields. The general picture that emerges is that VF-type macromolecules do obey scaling, fact with differentiates them from the dendrimers. Here, of course, also the question whether a Θ-point may be found is of much interest; at the Θ-point the structure should behave as an ideal one, given that the two-body interactions should, on the average, cancel exactly. Given, however, the complexity of the question (we note that even for stars and for dendrimers it is a matter of heated debate), the whole problem is an issue for additional studies. Evidently, structures build from very long spacer chains are more prone to behave in a Gaussian fashion.

In summary, we hope to have demonstrated that regular hyperbranched polymers may display very interesting mechanical and dielectric relaxation properties. Hence, we look forward to having substances with VF architecture soon synthesized, thus allowing for their experimental investigation.

Acknowledgment. We acknowledge gratefully the help of the Deutsche Forschungsgemeinschaft. A.B. thanks the Fonds der Chemischen Industrie and BMBF for their support.

Appendix

Here we present the details of the decimation procedure discussed in section 2. Our starting point is eq 6 or, explicitly, eqs 7−9, which give the relations between the components ϕ of the eigenvector $\mathbf{\Phi}$ belonging to a particular eigenvalue λ.

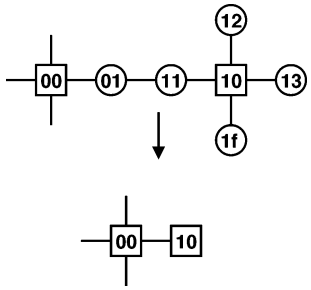

Figure 14. Decimation step for singly coordinated centers.

For a dangling end case, the situation is sketched in Figure 14. In this figure, the beads that get eliminated in the decimation step are shown as circles. The components corresponding to these beads are ϕ_{ij} with $1 \leq j \leq f$ and ϕ_{01}. Note that the figure is based on the special case $f = 4$ but that in the following derivation f is arbitrary, $f \geq 3$. The two beads shown as squares are those that remain after the decimation; their components are ϕ_{00} and ϕ_{10}. The eigenvalue equations for the considered components read, from eq 6

$$(1 - \lambda)\phi_{1j} = \phi_{10}, \quad \text{for } 2 \leq j \leq f \tag{51}$$

$$(f - \lambda)\phi_{10} = \phi_{11} + \sum_{j=2}^{f} \phi_{1f} \tag{52}$$

$$(2 - \lambda)\phi_{11} = \phi_{01} + \phi_{10} \tag{53}$$

and

$$(2 - \lambda)\phi_{01} = \phi_{00} + \phi_{11} \tag{54}$$

Now, eqs 53 and 54 can be combined, leading to

$$(2 - \lambda)^2\phi_{11} = (2 - \lambda)\phi_{10} + \phi_{00} + \phi_{11} \tag{55}$$

hence

$$\phi_{11} = [(2 - \lambda)^2 - 1]^{-1}\,[(2 - \lambda)\phi_{10} + \phi_{00}] \tag{56}$$

On the other hand, from eq 51, one has simply

$$\phi_{1j} = (1 - \lambda)^{-1}\phi_{10}, \quad \text{for } 2 \leq j \leq f \tag{57}$$

Inserting eq 56 and 57 into eq 52 leads to

$$(f - \lambda)\phi_{10} = [(2 - \lambda)^2 - 1]^{-1}[(2 - \lambda)\phi_{10} + \phi_{00}] + (f - 1)(1 - \lambda)^{-1}\phi_{10} \tag{58}$$

hence

$$\phi_{00} = \{[(2 - \lambda)^2 - 1][(f - \lambda) - (f - 1)(1 - \lambda)^{-1}] - (2 - \lambda)\}\phi_{10} \tag{59}$$

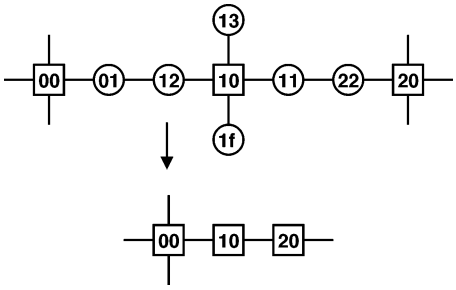

Figure 15. Decimation step for doubly coordinated centers.

Remarking that $[(2-\lambda)^2-1]=\lambda^2-4\lambda+3=(1-\lambda)(3-\lambda)$, it is now straightforward to verify that eq 59 can be reformulated in terms of $P(\lambda)$, eq 13 as

$$\phi_{00}=[1-P(\lambda)]\phi_{10} \tag{60}$$

which corresponds to eq 12 of the main text.

The procedure is straightforwardly extended to the other two cases, involving two- and *f*-coordinated beads. The situation for 2-fold coordination is shown in Figure 15. Here, the components of the circular beads to be eliminated are ϕ_{01} and ϕ_{22}, as well as ϕ_{1j} with $1 \le j \le f$. The components of the three square beads that remain after decimation are ϕ_{00}, ϕ_{10}, and ϕ_{20}. The eigenvalue equations for the components read

$$(2-\lambda)\phi_{01}=\phi_{00}+\phi_{12} \tag{61}$$

$$(2-\lambda)\phi_{12}=\phi_{01}+\phi_{10} \tag{62}$$

$$(1-\lambda)\phi_{1j}=\phi_{10}, \quad \text{for } 3 \le j \le f \tag{63}$$

$$(f-\lambda)\phi_{10}=\phi_{11}+\phi_{12}+(f-2)\phi_{13} \tag{64}$$

$$(2-\lambda)\phi_{11}=\phi_{10}+\phi_{22} \tag{65}$$

and

$$(2-\lambda)\phi_{22}=\phi_{20}+\phi_{11} \tag{66}$$

As before, eqs 61 and 62 on one hand and eqs 65 and 66 on the other hand can be combined, leading to

$$\phi_{12}=[(2-\lambda)^2-1]^{-1}[(2-\lambda)\phi_{10}+\phi_{00}] \tag{67}$$

and to

$$\phi_{11}=[(2-\lambda)^2-1]^{-1}[(2-\lambda)\phi_{10}+\phi_{20}] \tag{68}$$

respectively. On the other hand, eq 63 gives

$$\phi_{1j}=(1-\lambda)^{-1}\phi_{10}, \quad \text{for } 3 \le j \le f \tag{69}$$

Inserting eqs 67 to 69 into eq 64 leads to

$$(f-\lambda)\phi_{10}=[(2-\lambda)^2-1]^{-1}[2(2-\lambda)\phi_{10}+\phi_{00}+\phi_{20}]+(f-2)(1-\lambda)^{-1}\phi_{10} \tag{70}$$

Hence

$$\phi_{00}+\phi_{20}=\{[(2-\lambda)^2-1][(f-\lambda)-(f-2)(1-\lambda)^{-1}]-2(2-\lambda)\}\phi_{10} \tag{71}$$

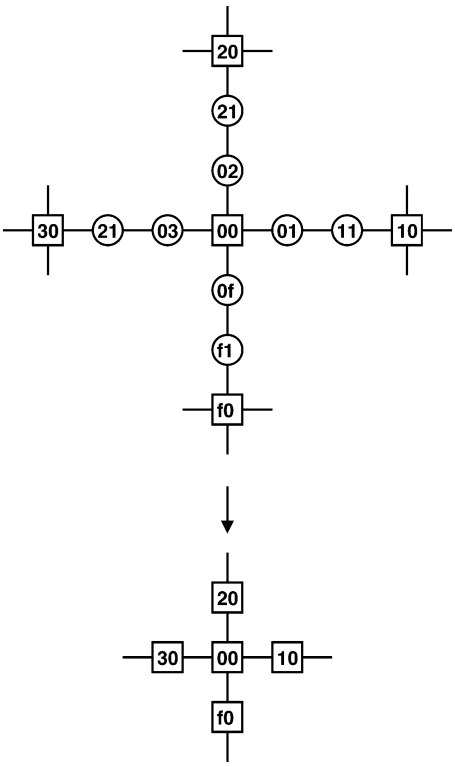

Figure 16. Decimation step for *f*-coordinated centers.

which reformulated in terms of $P(\lambda)$ reads

$$\phi_{00}+\phi_{20}=[2-P(\lambda)]\phi_{10} \tag{72}$$

corresponding to eq 11 of the main text.

The situation for the *f* coordinated beads is shown in Figure 16 and it is even simpler, since no dangling bead reduction has to be taken care of in this case. The components of the circular beads to be eliminated are now ϕ_{0j} and ϕ_{j1}, with $1 \le j \le f$, while the components of the remaining square beads are ϕ_{k0} with $0 \le k \le f$. The eigenvalue equations for these components read

$$(2-\lambda)\phi_{j1}=\phi_{0j}+\phi_{j0}, \quad \text{for } 1 \le j \le f \tag{73}$$

$$(2-\lambda)\phi_{0j}=\phi_{00}+\phi_{j1}, \quad \text{for } 1 \le j \le f \tag{74}$$

and

$$(f-\lambda)\phi_{00}=\sum_{j=1}^{f}\phi_{0j} \tag{75}$$

As before, eqs 73 and 74 yield

$$\phi_{0j}=[(2-\lambda)^2-1]^{-1}[(2-\lambda)\phi_{00}+\phi_{j0}], \quad \text{for } 1 \le j \le f \tag{76}$$

Finally, inserting eq 76 into eq 75 leads to

$$(f-\lambda)\phi_{00}=[(2-\lambda)^2-1]^{-1}[f(2-\lambda)\phi_{00}+\sum_{j=1}^{f}\phi_{j0}] \tag{77}$$

Hence

$$\sum_{j=1}^{f}\phi_{j0}=\{[(2-\lambda)^2-1](f-\lambda)-f(2-\lambda)\}\phi_{00} \tag{78}$$

or, reformulated

$$\sum_{j=1}^{f} \phi_{j0} = [f - P(\lambda)]\phi_{00} \tag{79}$$

which corresponds to eq 10 of the main text.

As a last comment, we note that eqs 57 and 69 require that $\lambda \neq 1$; otherwise the fCC to which the dangling modes are attached do not move. Then the modes around such fCC are localized, see eqs 52 and 64. This leads, as we proceed to show, to the degeneracy mentioned in the main text, eq 22, where we obtain Δ_g by counting all the linearly independent modes in which the fCC are immobile.

In the recursive construction of VF, the number of fCCs increases by a factor $f + 1$ at each generation, so that the number of fCCs at generation g is $(f + 1)^{g-1}$. Because of eq 8, each of the pairs of intermediate beads connecting any two fCCs must move in parallel. For a connected local mode, we define its origin as the fCC with moving neighboring beads which is closest to the center of the VF. We may now select a complete set of linearly independent modes by requiring that any mode of the set has next to such a fCC exactly two beads that move antisymmetrically. Then, each fCC of the VF is origin to $f - 2$ of these modes, unless it is the central fCC, which is origin to $f - 1$ modes of the set. Taking care of the one additional mode for the central fCC, we find that

$$\Delta_g = (f - 2)(f + 1)^{g-1} + 1 \tag{80}$$

which is eq 22 of the main text.

References and Notes

(1) Rouse, P. E. *J. Chem. Phys.* **1953**, *21*, 1272.
(2) Zimm, B. H. *J. Chem. Phys.* **1956**, *24*, 269.
(3) Roovers, J. In *Star and Hyperbranched Polymers*; Mishra, M. K., Kobayashi, S., Eds.; Marcel Dekker: New York, 1999; p 285.
(4) Roovers, J.; Comanita, B. *Adv. Polym. Sci.* **1999**, *142*, 179.
(5) Cai, C.; Chen, Z. Y. *Macromolecules* **1997**, *30*, 5104.
(6) Chen, Z. Y.; Cai, C. *Macromolecules* **1999**, *32*, 5423.
(7) Ganazzoli, F.; La Ferla, R.; Raffaini, G. *Macromolecules* **2001**, *34*, 4222.
(8) Burchard, W. *Adv. Polym. Sci.* **1999**, *143*, 113.
(9) Freire, J. J. *Adv. Polym. Sci.* **1999**, *143*, 35.
(10) Kemp, J.; Chen, Z. Y. *Phys. Rev. E* **1997**, *56*, 7017.
(11) Denneman, A. I. M.; Jongschaap, R. J. J.; Mellema, J. *J. Chem. Phys.* **1999**, *111*, 8182.
(12) Gurtovenko, A. A.; Gotlib, Yu. Ya. *Macromolecules* **1998**, *31*, 5756.
(13) Gurtovenko, A. A.; Gotlib, Yu. Ya. *Macromolecules* **2000**, *33*, 6578.
(14) Gurtovenko, A. A.; Blumen, A. *J. Chem. Phys.* **2001**, *115*, 4924.
(15) Doi, M.; Edwards, S. F. *The Theory of Polymer Dynamics*; Clarendon Press: Oxford, England, 1986.
(16) Grosberg, A. Yu.; Khokhlov, A. R. *Statistical Physics of Macromolecules*; AIP Press: New York, 1994.
(17) Sommer, J.-U.; Blumen, A. *J. Phys. A* **1995**, *28*, 6669.
(18) Biswas, P.; Kant, R.; Blumen, A. *Macromol. Theory Simul.* **2000**, *9*, 56.
(19) Kant, R.; Biswas, P.; Blumen, A. *Macromol. Theory Simul.* **2000**, *9*, 608.
(20) Biswas, P.; Kant, R.; Blumen, A. *J. Chem. Phys.* **2001**, *114*, 2430.
(21) von Ferber, C.; Blumen, A. *J. Chem. Phys.* **2002**, *116*, 8616.
(22) Vicsek, T. *Fractal Growth Phenomena*; World Scientific: Singapore, 1989.
(23) Jayanthi, C. S.; Wu, S. Y.; Cocks, J. *Phys. Rev. Lett.* **1992**, *69*, 1955.
(24) Jayanthi, C. S.; Wu, S. Y. *Phys. Rev. B* **1993**, *48*, 10188.
(25) Jayanthi, C. S.; Wu, S. Y. *Phys. Rev. B* **1993**, *48*, 10199.
(26) Jayanthi, C. S.; Wu, S. Y. *Phys. Rev. B* **1994**, *50*, 897.
(27) Blumen, A.; Jurjiu, A. *J. Chem. Phys.* **2002**, *116*, 2636.
(28) Jurjiu, A.; Friedrich, Ch.; Blumen, A. *Chem. Phys.* **2002**, *284*, 221.
(29) Cates, M. E. *Phys. Rev. Lett.* **1984**, *53*, 926.
(30) Cates, M. E. *J. Phys. (Fr.)* **1985**, *46*, 1059.
(31) Friedrich, Ch.; Schiessel, H.; Blumen, A. In *Advances in the Flow and Rheology of Non-Newtonian Fluids*; Siginer, D. A., DeKee, D., Chhabra, R. P., Eds.; Elsevier, Amsterdam, 1999; p 429ff.
(32) Schiessel, H. *Phys. Rev. E* **1998**, *57*, R5775.
(33) Schiessel, H.; Friedrich, Ch.; Blumen, A. In *Applications of Fractional Calculus in Physics*; Hilfer, R., Ed.; World Scientific: Singapore, 2000; p 331.
(34) Sokolov, I. M.; Klafter, J.; Blumen, A. *Phys. Today* **2002**, p 48.
(35) Schwalm, W. A.; Schwalm, M. K.; Giona, M. *Phys. Rev. E* **1997**, *55*, 6741.
(36) Bronstein, I. N.; Semendjajev, K. A. *Taschenbuch der Mathematik (Handbook of Mathematics)*; Nauka and Teubner: Moscow and Leipzig, Germany, 1985; Chapter 2.4.2.
(37) Lach, C.; Müller, P.; Frey, H.; Mülhaupt, R. *Macromol. Rapid Commun.* **1997**, *18*, 253. Frey, H.; Lach, C.; Schlenk, C.; Pusel, T. *Polym. Prepr.* **2000**, *41*, 568.
(38) Möck, A.; Burgath, A.; Hanselmann, R.; Frey, H. *Macromolecules* **2001**, *34*, 7692; Möck, A.; Burgath, A.; Hanselmann, R.; Frey, H. *Polym. Mater. Sci. Eng.* **1999**, *80*, 173; Burgath, A.; Möck, A.; Hanselmann, R.; Frey, H. *Polym. Mater. Sci. Eng.* **1999**, *80*, 126.
(39) Lambert, C.; Nöll, G. *J. Am. Chem. Soc.* **1999**, *121*, 8434. Lambert, C. *J. Chem. Soc., Perkin Trans.* **1999**, *2*, 577.
(40) Lambert, C.; Nöll, G. *Synth. Met.* **2003**, *139*, 57.
(41) Lambert, C.; Nöll, G. *Chem.—Eur. J.* **2002**, *8*, 3467.
(42) Casewit, C. J.; Colwell, K. S.; Rappe, A. K. *J. Am. Chem. Soc.* **1992**, *114*, 10035; —, *J. Am. Chem. Soc.* **1992**, *114*, 10046.
(43) Domany, E.; Alexander, S.; Bensimon, D.; Kadanoff, L. P. *Phys. Rev. B* **1983**, *28*, 3110.
(44) Rammal, R. *J. Phys. (Fr.)* **1984**, *45*, 191.
(45) Kirkwood, J. G.; Riseman, J. *J. Chem. Phys.* **1948**, *16*, 565.
(46) Rotne, J.; Prager, S. *J. Chem. Phys.* **1969**, *50*, 4831.
(47) Ward, I. M. *Mechanical Properties of Solid Polymers*, 2nd ed.; J. Wiley & Sons: Chichester, England, 1985.
(48) Ferry, J. D. *Viscoelastic Properties of Polymers*, 3rd ed.; J. Wiley & Sons: New York, 1980.
(49) Gurtovenko, A. A.; Gotlib, Yu. Ya.; Blumen, A. *Macromolecules* **2002**, *35*, 7481.
(50) Williams, G. *Chem. Rev.* **1972**, *72*, 55.
(51) Stockmayer, W. H.; Baur, M. E. *J. Am. Chem. Soc.* **1964**, *86*, 3485.
(52) Stockmayer, W. H. *Pure Appl. Chem.* **1967**, *15*, 539.
(53) Yamakawa, H. *Modern Theory of Polymer Solutions*; Harper and Row: New York, 1971.
(54) Gurtovenko, A. A.; Blumen, A. *Macromolecules* **2002**, *35*, 3288.
(55) Perkins, T. T.; Smith, D. E.; Larson, R. G.; Chu, S. *Science* **1995**, *268*, 83.
(56) Wirtz, D. *Phys. Rev. Lett.* **1995**, *75*, 2436.
(57) Quake, S. R.; Babcock, H.; Chu, S. *Nature* **1997**, *388*, 151.
(58) Amblard, F.; Maggs, A. C.; Yurke, B.; Pergellis, A. N.; Leibler, S. *Phys. Rev. Lett.* **1996**, *77*, 4470.
(59) Hatfield, J. W.; Quake, S. R. *Phys. Rev. Lett.* **1999**, *82*, 3548.
(60) Helfer, E.; Harlepp, S.; Bourdieu, L.; Robert, J.; MacKintosh, F. C.; Chatenay, D. *Phys. Rev. Lett.* **2000**, *85*, 457.
(61) Klafter, J.; Blumen, A. *J. Chem. Phys.* **1984**, *80*, 875.
(62) Colby, R. H.; Gillmor, J. R.; Rubinstein, M. *Phys. Rev. E* **1993**, *48*, 3712.
(63) Rubinstein, M.; Colby, R. H. *Macromolecules* **1994**, *27*, 3184.
(64) Heinrich, G.; Vilgis, T. A. *Europhys. Lett.* **1994**, *25*, 175.
(65) Trautenberg, H. L.; Sommer, J.-U.; Göritz, D. *J. Chem. Soc., Faraday Trans.* **1995**, *91*, 2649.
(66) Huber, G.; Vilgis, T. A.; Heinrich, G. *J. Phys. C* **1996**, *8*, L 409.
(67) Bunde, A.; Havlin, S. Eds. *Fractals and Disordered Systems*; Springer-Verlag: Berlin, 1996.
(68) Granek, R.; Klafter, J. *Europhys. Lett.* **2001**, *56*, 15.

(69) La Ferla, R. *J. Chem. Phys.* **1997**, *106*, 688.
(70) Smith, B. T.; Boyle, J. M.; Dongarra, J. J.; Garbow, B. S.; Ikebe, Y.; Klema, V. C.; Moler, C. B. *Matrix Eigensystem Routines − EISPACK Guide*, *Lecture Notes in Computer Science*; Springer: Berlin, 1976; Vol. 6.
(71) Garbow, B. S.; Boyle, J. M.; Dongarra, J. J.; Moler, C. B. *Matrix Eigensystem Routines − EISPACK Guide Extension*, *Lecture Notes in Computer Science*; Springer: Berlin, 1977; Vol. 51.
(72) Bunch, J.; Dongarra, J.; Moler, C.; Stewart, G. W. *LINPACK User's Guide*; SIAM: Philadelphia, PA, 1979.
(73) Jurjiu, A.; Koslowski, Th.; Blumen, A. *J. Chem. Phys.* **2003**, *118*, 2398.
(74) Koslowski, Th.; von Niessen, W. *J. Comput. Chem.* **1993**, *14*, 769.
(75) Lanczos, C. *J. Res. NBS B* **1950**, *45*, 225.
(76) Cullum, J. K.; Willoughby, R. *Lanczos Algorithms for Large Symmetric Eigenvalue Problems*; Birkhäuser: Boston, MA, Basel, Switzerland, and Stuttgart, Germany, 1985; Vol. I (Theory), Vol. II (Programs).

MA034553G